EUROFUSION WPMST1-PR(16) 14022

AV Bogomolov et al.

The effect of nitrogen seeding on ELM filaments

Preprint of Paper to be submitted for publication in
Nuclear Fusion

This work has been carried out within the framework of the EUROfusion Consortium and has received funding from the Euratom research and training programme 2014-2018 under grant agreement No 633053. The views and opinions expressed herein do not necessarily reflect those of the European Commission.

The effect of nitrogen seeding on ELM filaments

A V Bogomolov[1], I G J Classen[1], A J H Donné[1,2,3], M Dunne[4], P A Schneider[4], E Wolfrum[4], B Vanovac[1], R Fischer[4], L Frassinetti[5], N C Luhmann Jr.[6] and the ASDEX Upgrade Team, the EUROfusion MST1 Team*.

[1] *FOM-Institute DIFFER, Dutch Institute for Fundamental Energy Research, 5600 HH Eindhoven, The Netherlands*
[2] *Eindhoven University of Technology, 5600 MB Eindhoven, The Netherlands*
[3] *EUROfusion, Boltzmannstraße 2, 85748 Garching, Germany*
[4] *Max-Planck-Institut für Plasmaphysik, Boltzmannstraße 2, 85748 Garching, Germany*
[5] *Division of Fusion Plasma Physics, Association EUROATOM-VR, KTH, Sweden*
[6] *University of California at Davis, Davis, CA 95616, USA*

E-mail: A.Bogomolov@differ.nl

Abstract

The aim of this work is to study the effect of nitrogen gas puffing on Edge Localized Modes (ELMs). Nitrogen seeding reduces the ELM duration and often leads to the enhancement of the plasma confinement. One of the theoretical explanations of ELM reduction under effect of nitrogen are changes in the filamentary structure of ELMs. With the help of the Electron Cyclotron Emission Imaging (ECEI) diagnostic on the ASDEX-Upgrade (AUG) tokamak, experimental evidence for this hypothesis was obtained. It is shown that nitrogen seeded ELMs expel less filaments, the number of filaments in an ELM correlates well with both the duration of the ELM crash and the ELM-related pressure drop. The energy loss per filament event in the analysed shots is estimated as $2.5 - 5\,\mathrm{kJ}$.

(The figures in this article are in colour only in the electronic version)

*See http://www.euro-fusionscipub.org/mst1

1 Introduction

In discharges with high heating power the divertor loads limit the operation of AUG [1]. Impurity seeding can solve the problem by increasing the radiative power in the divertor. Different impurity gasses are used for increasing the radiative power: the effect of nitrogen, neon and argon was investigated on Alcator C-Mod [2], a comparison between neon, argon and krypton has been performed on DIII-D [3][4]. The most favourable gas for seeding is nitrogen, as it mostly radiates in the scrape-off layer (SOL) and divertor region [5][6], reducing the divertor power loads and allowing operation at higher core heating power [7].

Apart from preventing the divertor tiles from overheating, nitrogen seeding is often observed to improve confinement in devices with metallic walls, when puffed up to a certain flux [8]. On the Joint European Torus (JET) it is reported, that nitrogen improves confinement in the high-shape H-mode [9]. Studies pointed out that the improvement of confinement is most likely an edge effect [8], which is supported by the differences in the impact of nitrogen in case of the ITER-like wall (ILW) and carbon wall [10] as well as by strong changes in ELM behaviour. Typically, at a certain nitrogen seeding flux, ELM energy losses become lower, whereas the ELMs become more frequent. This effect has been extensively studied experimentally on AUG and JET [7][11][12][13][14][15]. Observations suggest, that nitrogen can indirectly change the ELM behaviour by reducing the SOL temperature [16]. Among other explanations, filamentary changes were proposed. Calculations with the non-linear magnetohydrodynamic (MHD) code JOREK performed for the Mega Amp Spherical Tokamak (MAST) [17] show that the dynamics of the filaments, which often accompany ELM crashes, is dependent on the temperature of the scrape-off layer.

The work presented in this article shows experimental evidence for changes in ELM filaments, which are directly related to the ELM energy loss. The filaments have been widely investigated by a variety of diagnostics on different machines: MAST [23][18][19][30], JET [20][21], C-MOD [22] and others [26]. In this paper the term 'filament' refers to relatively hot structures in comparison to the background, which appear after the ELM crash and that are elongated in the poloidal direction. Here the effect of nitrogen seeding on ELM filaments is studied by means of the Electron Cyclotron Emission Imaging (ECEI) diagnostic on AUG. The ECEI system at AUG is a 2D diagnostic which consists of a linear array of 16 detectors, looking at different vertical positions in the plasma. Each detector acts as a standard (1D) ECE radiometer with 8 radial channels. In total the ECEI diagnostic has 128 channels which cover an observational area of $\sim$10x40 cm^2 [25]. The diagnostic geometry in the

plasma is shown in Fig. 4(left). The ECEI system is cross-calibrated versus the absolutely calibrated 1D ECE system.

The paper is organized as follows. In section 2 the details of the experiment are given; the well-known evolution of ELMs under the effect of nitrogen seeding is described. Section 3 is dedicated to studying the relation between the ELM duration and its filaments; ELM cycle phases are introduced. Section 4 shows an ELM precursor, which typically accompanies nitrogen seeded ELMs. Characteristics of the precursor are given. In section 5 the plasma kinetic profiles are compared for nitrogen seeded and non-seeded ELMs. A summary is given in section 5.

2 Evolution of ELMs during nitrogen seeding

Puffing a sufficient amount of nitrogen into the plasma ($\sim$ 12% of the deuterium gas puff rate) leads to changes in the ELM behaviour [7][14]. An evolution of some ELM properties under N_2 puffing is shown in Fig. 1, representing AUG discharge #30417. In this discharge the nitrogen is puffed in two steps: the puff starts with a rate of $1.4 \cdot 10^{21}\,\mathrm{e^-\,s^{-1}}$ at 2.3 s, which is then increased up to $3.0 \cdot 10^{21}\,\mathrm{e^-\,s^{-1}}$ after 3.2 s. In order to maintain the same amount of nitrogen and taking into account its accumulation in the plasma, the puffing rate slightly decreases between the steps. Other discharge parameters are as follows: $B_t = -2.5\,\mathrm{T}$, $I_p = 1.0\,\mathrm{MA}$, $P_{\mathrm{NBI}} = 12\,\mathrm{MW}$ after 2.1 s, $P_{\mathrm{ECRH}} = 1.7\,\mathrm{MW}$, $P_{\mathrm{ICRH}} = 2.0\,\mathrm{MW}$. The analysis in this paper is based on four nitrogen-seeded discharges with a common feature of high NBI heating power of 12 MW. The choice for high heating power was made because the modes are better seen by ECEI.

Fig. 1b shows the nitrogen puff together with the divertor thermal current. The divertor thermal current is a current produced by temperature differences between inner and outer divertor plates via sheath potential differences [28]. It is proportional to the thermal loads experienced by the divertor and can be used to obtain the ELM frequency f_{ELM} and ELM duration τ_{ELM}. Here the ELM duration is determined by setting a threshold on the divertor current: the time when the divertor current is higher than the threshold is considered as the ELM duration. From Fig. 1d it is seen that the ELMs can be separated in two groups according to their duration: a 'long' ELMs group, which have a duration in the range of $2-3\,\mathrm{ms}$ (red stars) and a 'short' ELMs group (green circles), which have a duration of about 1 ms. In the absence of nitrogen or with slight nitrogen seeding both groups simultaneously coexist with the long ELMs prevailing.

Before the nitrogen puff begins, the plasma is in a type-I ELMy H-mode,

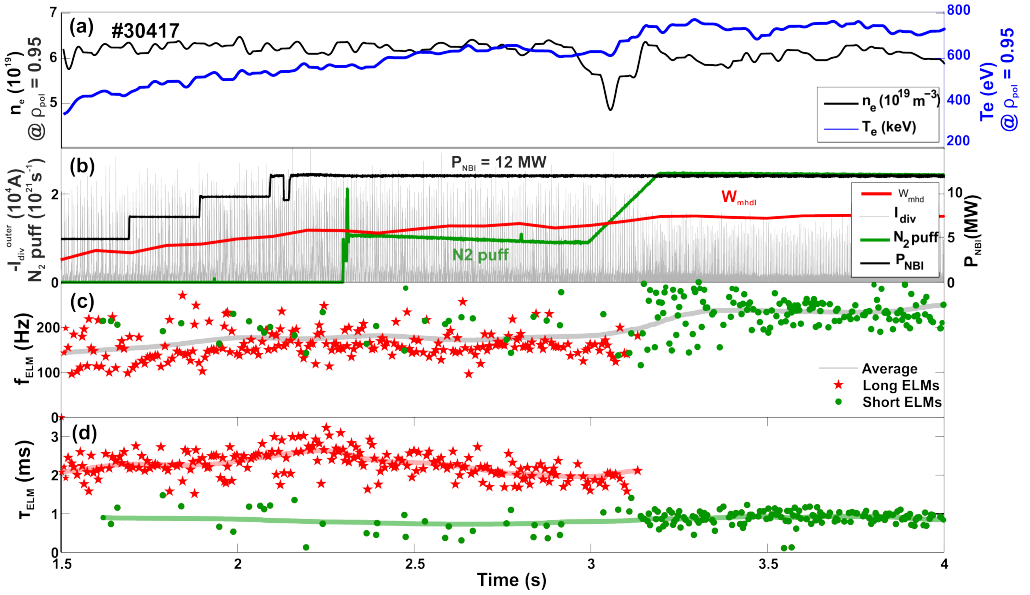

Figure 1: ELM frequency evolution related to the nitrogen seeding for AUG discharge #30417. a) Density and temperature timetraces (smoothed) taken at $\rho_{\mathrm{pol}} = 0.95$. b) Divertor thermal current, NBI power, total stored energy W_{mhd} and nitrogen puff rate. With the second step of the nitrogen puff ELMs become smaller. c) ELM frequency f_{ELM}. The ELM frequency slowly increases after the second step of the nitrogen puff. d) ELM duration τ_{ELM}. The ELMs with a duration of more than 1.5 ms are considered to be 'long' and are marked with red stars, while the ones with a duration of less than 1.5 ms are 'short' and are marked with the green dots. Both types can coexist at the same time. The curves in bold are a guide to the eye indicating the average.

with the ELM frequency, calculated as the inverse of the inter-ELM period, around $100 - 150$ kHz (Fig. 1c). At 2.3 s the first step of the N_2 puff begins. Due to the low puffing rate, it does not lead to significant changes in the ELM behaviour, however, the total stored energy W_{mhd} slightly increases. After the second step which starts at 3.0 s, the ELMs change significantly: long ELMs completely disappear, substituted by short ELMs with a higher frequency of $200 - 250$ kHz. With the higher nitrogen puff W_{mhd} also continues to grow. Fig. 2 shows the duration distribution of the ELMs in the discharge, showing a clear separation between the two ELM groups. The transition from the long ELMs regime to the short ELMs regime is very sharp. Either it is a very steep function of the amount of nitrogen, or there is a threshold behaviour in its nature.

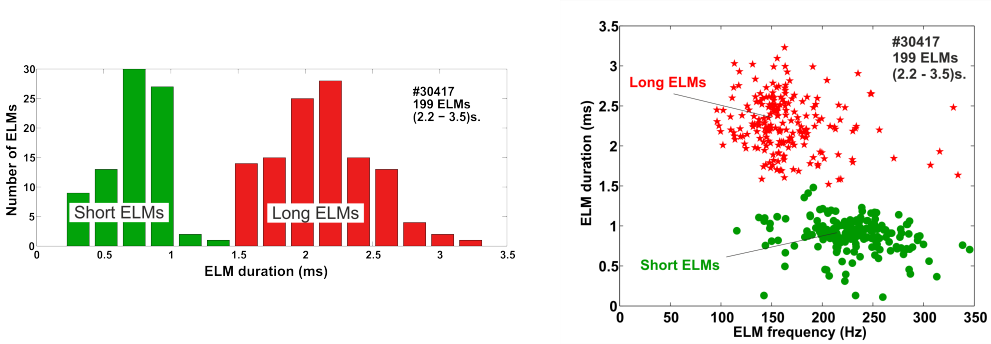

Figure 2: Left: ELM frequency distribution along discharge #30417, calculated for all the ELMs in the time interval between 2.2 and 3.5 s. Right: ELM duration as a function of ELM frequency. Short ELMs are mostly associated with the strong nitrogen seeding.

3 ELM duration and filaments

The comparison between the short ELMs in the presence of nitrogen and the conventional type-I ELMs was performed on AUG by Schneider et al. and presented in ref. [13]. Three different phases of an ELM cycle have been identified (see Fig. 3). (I) The ELM crash itself with two subphases: (Ia) the rise of the divertor thermal current signal, (Ib) the flat phase of the divertor current; (II) the decay of the divertor current, (III) the inter-ELM phase, during which the pedestal parameters begin to recover [13].

Short nitrogen seeded ELMs differ from type-I ELMs by the absence of the (Ib) phase, where the divertor current is flat. Instead, in the case of short ELMs, the divertor current starts to fall immediately after the rise, thereby skipping the flat phase (see Fig. 3). Skipping the (Ib) phase makes nitrogen seeded ELMs to be on average 1 ms shorter than type-I ELMs.

With the ECEI diagnostic it is possible to observe what is happening during the (Ib) phase, which allows to find out other principal differences between type-I ELMs and nitrogen seeded ELMs.

Fig. 3 shows a conventional type-I ELM (a, b, c, d) and a short nitrogen seeded ELM (d, e, f, g), as seen by the divertor current (a, e) and the ECEI. The ECEI data is presented in two different ways: as signals from two single channels (b, f) and as 2D data arrays of vertical chords (c, d; g, h). A pair of channels or chords represent the data measured inside (c, g) and outside (d, h) of the separatrix. A short discussion on the position of the ECEI channels relative to the separatrix is given below. Due to the curvature of the magnetic field (Fig. 4) some channels of a vertical chord are exposed to higher temperatures than others, as they are closer to the plasma center.

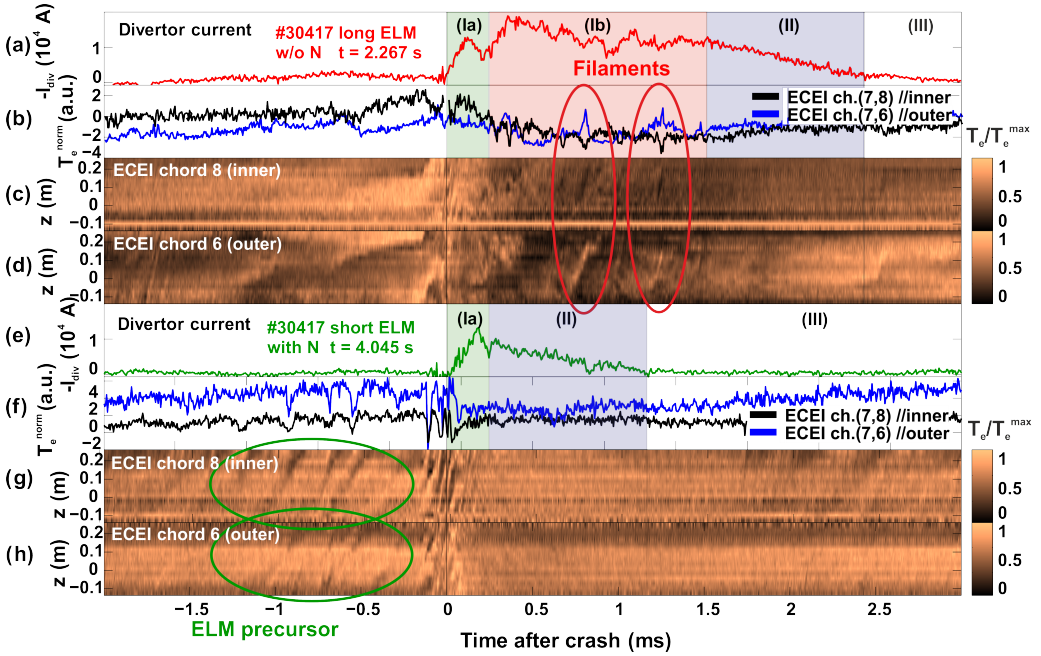

Figure 3: Long (in red) and short (N_2 seeded, in green) ELMs as seen by the divertor current (a, e) and ECE Imaging (b, c, d, f, g, h). Phase (I): the ELM onset and development. Long ELMs have an additional (Ib) phase, during which filaments are produced, not present in short ELMs. Phase (II): the decay of the ELM crash. Phase (III): the recovery of the pedestal. a) Divertor current for an ELM without nitrogen. b) Two ECEI channels (7,8) and (7,6), with the first located inside and the second outside the separatrix. Temperature rise for the inner channel and drops for the outer one related to filaments are marked by red ellipses. c) ECEI inner vertical chord. d) ECEI outer vertical chord. e) Divertor current for a nitrogen seeded ELM. f) Two ECEI channels: the inner one (7,8) and the outer one (7,6). g) ECEI inner vertical chord for the case of a nitrogen seeded ELM. An ELM precursor is marked with the green ellipses. h) ECEI outer vertical chord of the nitrogen seeded ELM. The ECEI is cross-calibrated versus the absolutely calibrated 1D ECE.

As here the relative temperature fluctuations are more important than the absolute ones, each of the ECEI channels is separately normalized to the same amplitude level. The time traces of the single ECEI channels (b, f) are normalized to their average values across the whole discharge. There are two principal differences observed by ECEI between the conventional type-I ELMs and short nitrogen seeded ELMs. One of them is that the nitrogen seeded ELMs have a strong precursor (Fig. 3g,h, the green ellipse), which is

not commonly seen in case of type-I ELMs. This difference will be considered in more detail in section 4. Here another difference will be discussed: the existence of filaments, which are typically produced after type-I ELM crashes (Fig. 3b,c,d), and which do not occur after nitrogen seeded ELMs.

As was mentioned before, in this paper the term 'filament' refers to relatively hot structures in comparison to the background, which appear after the ELM crash. These structures, opposite to the coherent and regular ELM onset modes (described, for instance, in [24]), are singular events and, according to the resonance positions of the ECEI not taking the shine through into account, are only observed outside the separatrix (see Fig. 3cd, Fig. 4). The filaments, accompanying type-I ELMs on AUG, are usually produced in bursts and have the following characteristics: rotation mostly in the electron diamagnetic drift direction with typical velocities of 2 km/s, the filaments are usually produced within 3 ms after a crash, and can have a temperature of up to 200 eV [27]. Note that all ECEI measurements are taken in the laboratory frame, which is a sum of the fluctuation velocity itself and the plasma $E \times B$ rotation velocity: $V_{\mathrm{LAB}} = \omega/k + V_{E\times B}$. With the help of ECEI it is possible to count the number of filaments which are produced after each ELM and which pass through the ECEI observation window. The filaments in Fig. 3c are seen as dark inclined lines, indicating that the temperature inside the separatrix locally drops (Fig. 3b), whereas on the outer channels (Fig. 3d) the filaments appear as bright lines, locally increasing the temperature as they are being produced. One of the filaments caught in Fig. 3 is shown in 2D in Fig. 4, where three snapshots of the filament are represented.

Before making some statistics on the filaments, one should address an issue related to the fraction of all filaments seen by ECEI.

A typical filament seen by the ECEI on AUG has the lifetime comparable with its observation time: $\sim 250\,\mu$s and the poloidal velocity about 2 km/s. The magnetic field line inclination $B_t/B_p \sim 4$ at the position of the ECEI viewing window. Considering filaments to be elongated along the magnetic field lines, each filament crosses at some toroidal location the mid-plane. Filaments crossing the mid-plane no further than 80 cm left or right of the ECEI viewing window will be seen by the diagnostic (the view extends 20 cm above and below the mid-plane which, due to the pitch of the field lines, corresponds to 80 cm left and right in the toroidal direction). On top of that, filaments that are born on the toroidal mid-plane location not further than 240 cm to the right will, due to their lifetime, rotate in view of ECEI window before they die (they are born 40 cm below the vertical view of ECEI and rotate ~ 40 cm upwards during their lifetime). Hence, the system is able to see the filaments which are born on a 320 cm toroidal section of the mid-plane (from 80 cm left to 240 cm right).

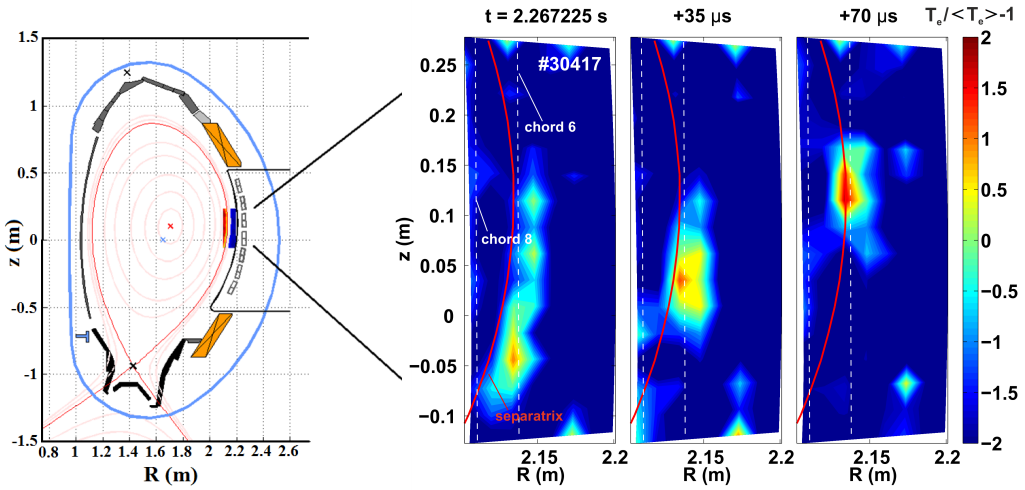

Figure 4: Left: ECEI observational area on AUG. An array of 16x8 channels covers $\sim$ 10x40 cm^2 of plasma. Right: three snapshots of a filament produced after a type-I ELM as seen by ECEI. The filament propagates poloidally in the electron diamagnetic drift direction slightly outside of the separatrix.

Taking into account, that the circumference at the low field side (LFS) of AUG is 13.5 m, the fraction of the filaments seen by ECEI is approximately 24% (3.2 m/13.5 m). In the present research the plots below are based on the number of filaments observed by ECEI, whereas in reality their number is four times higher.

Another issue related to filaments is that due to limitations of ECEI only filaments with high enough density (optically thick) and a size larger than 2.5 cm^2 can be seen. In Fig. 4 on the right the filament is observed outside the separatrix and it rotates in the electron diamagnetic drift direction in the laboratory frame, whereas filament-like structures on AUG have been previously reported to be rotating in the ion diamagnetic drift direction if they are outside of the separatrix [36]. However, it should be noted, that the term 'filament' is quite vague and various events can be brought under this definition. The position of the ECEI channels is strongly affected by the optical thickness of plasma, which may result in a difference between the true location of the filament and the corresponding emission peak, seen by ECEI (in Fig. 4, right). As the consequence, the filaments observed by the ECEI outside the separatrix could be actually situated slightly inside of it.

It is observed that the ELM duration τ_{ELM} correlates with the number of detected filaments produced after the crash. Fig. 5a shows this dependency for discharge #30423. Here ELMs with a duration $\tau_{\mathrm{ELM}} < 1.5$ ms are considered

to be short (see Fig. 2 for reference) and are marked by the green dots. Short ELMs never have more than one filament and in most cases they have no filaments at all. The ELMs with only one filament have the largest scatter in the duration time. The ELMs which produce two filaments or more are always long.

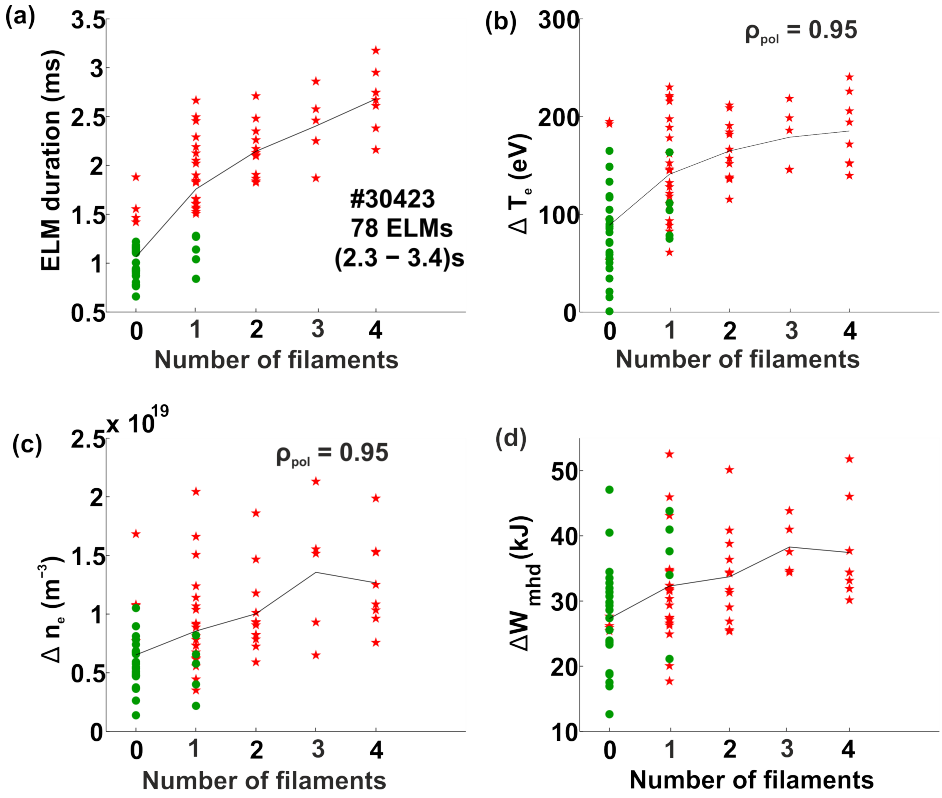

Figure 5: The effect of filaments on: a) ELM duration b) Electron temperature drop c) Density drop d) Plasma stored energy (W_{MHD}) drop. Long ELMs are marked with the red stars, short ELMs are marked with the green dots. Short ELMs do not expel more than one filament and, on average, cause a smaller temperature and density drop than long ELMs. The lines are a guide to the eye regarding the mean values.

There is also a correlation between the number of filaments and both the temperature and density drop, caused by an ELM. Fig. 5b,c shows these dependencies, with the temperature and density drops taken at $\rho_{\mathrm{pol}} = 0.95$. The values of the temperature and the density are provided by integrated data analysis (IDA) [37]. The ELMs which, according to IDA or the W_{mhd} signal, have shown a negative energy drop or temperature drop were excluded

from the data set. As a consequence of the correlation between the number of filaments and the pressure drop, the number of filaments correlates as well with the drop in the total stored energy W_{mhd}, shown in Fig. 5d. From the figure it is seen, that in discharge #30423 the average energy drop caused by type-I ELMs without filaments is about 27 kJ, while for the ELMs with four filaments the drop becomes ~ 37 kJ. This allows to estimate an average energy loss per filament event as 2.5 kJ. Hereafter, by a 'filament event' it is implied that there are also some non-filamentary losses possible, rather than the whole energy loss being caused by the filament itself. The obtained value of the energy loss per filament event is about 7% of the whole ELM energy loss, which is higher than for MAST or JET where it was estimated as 2.5% [29][21][30]. However, the fraction of the energy loss due to filaments here is about 25% of the total energy loss due to the ELM, which is in agreement with the energy arriving at the first wall on AUG [32] and is similar to the values on MAST and JET (30%) [31]. The discrepancy in the energy loss for a single filament event can come from either non-filamentary losses implicitly included in the current calculations, or from underestimation of total amount of filaments, as some of them can pass outside of the ECEI viewing window, as discussed above. Another possibility of the discrepancy is in the studied phenomena itself: on MAST and JET the filaments were studied which lead to the ELM crash, whereas here we are interested in the filaments which occur after an ELM crash.

Although, the scatter is rather high, the ELMs with two or more filaments have a tendency to reduce the plasma kinetic profiles more than the ELMs with only one filament or with no filaments at all. The latter ones can even have almost no effect on the profiles. The effect of different ELMs on the plasma kinetic profiles will be considered in section 5.

According to JOREK simulations performed by Pamela et al. [17], the SOL temperature can indirectly change the filament behaviour by affecting both plasma viscosity and resistivity. Particularly it was found that lower SOL temperatures lead a to lower number of filaments ejected. As it was experimentally shown by Fuchs et al. in ref. [6], nitrogen seeding enhances the radiation around the X-point, which reduces the temperature in the SOL relative to non-seeded discharges. The current research indicates, that the ELM duration is correlated with the number of filaments. Summarizing, a possible model can be the following: nitrogen reduces the SOL temperature, which indirectly, by increasing the plasma viscosity and resistivity, reduces the number of produced filaments by ELMs. The number of produced filaments is strongly correlated to the ELM length, which becomes shorter with the nitrogen seeding.

4 ELM precursors

As was mentioned in section 3, a typical feature of nitrogen-seeded ELMs observed on AUG is the presence of an ELM precursor mode. As currently presented work is based on four high power discharges, there is no evidence that the precursor mode will have the same characteristics in all other discharges. However, in this section some features of the ELM precursor modes, which are typical at least for high power discharges, will be analysed. In Fig. 3g the mode, which appears a few milliseconds before the crash, is the ELM precursor mode. The ELM precursor mode should not be confused to the coherent temperature fluctuations during the ELM onset, leading to the crash (described, for instance, in ref. [31]); those last not more than a few hundred microseconds, have high toroidal mode number n and appear directly prior to the crash. Here by 'precursor' a relatively long living ($2-3\,\mathrm{ms}$) mode is meant, which also appears as coherent temperature fluctuation and in the end merges into an ELM onset. This mode typically appears 2 ms after the previous nitrogen-seeded ELM. Note, that some temperature fluctuations can occur prior to conventional type-I ELM crashes as well (e.g. in Fig. 3d some bright structure prior to crash is observed), however, those do not have a regular structure or reproducibility from ELM to ELM. The precursors for the case of nitrogen seeded ELMs are highly reproducible and have a regular structure.

The N_2 ELM precursor mode differs significantly from the inter-ELM mode, described in ref. [34][33][35]. First of all, its mode frequency is in the order of several kHz (see Fig. 6b) compared to $20-50\,\mathrm{kHz}$ [35] for the inter-ELM mode. The second difference is that it always leads to a crash, while the inter-ELM mode can appear and also disappear in between two crashes. The nitrogen-seeded ELM precursor mode always disappears after the crash, while the inter-ELM mode can still be present in the background even after the ELM crash.

More detailed information on the N_2 ELM precursor mode can be obtained from Fig. 6, which shows the conditionally averaged mode velocity related to the averaged N_2-seeded ELM crash in the top plot and the corresponding conditionally averaged spectrogram of the ECEI channels in the bottom.

Fig. 6a is constructed as follows. Data, covering a time range from 4 ms pre-crash to 4 ms after it, is taken for each ELM. These data are then divided into samples of $80\,\mu\mathrm{s}$ and in each of them a 2D FFT is performed. After integrating the intensity of each 2D FFT over different frequencies ω and wave-numbers k, the velocity $V=\omega/k$ for each sample can be obtained which is then plotted explicitly. Positive values of the velocity correspond to mode rotation in the electron diamagnetic drift direction in the laboratory frame.

More details concerning this method can be found in ref. [33].

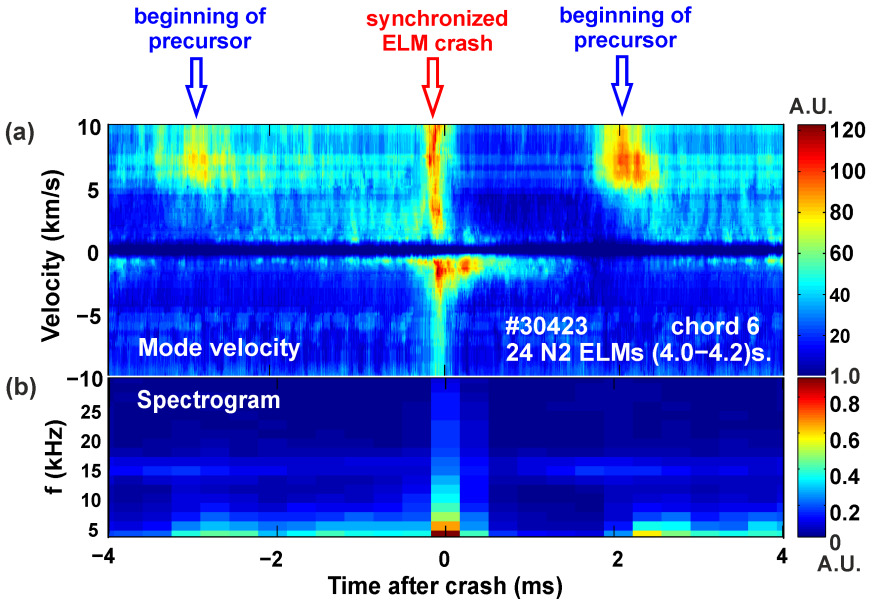

Figure 6: a) Conditionally averaged mode velocity for 24 nitrogen seeded ELMs in discharge #30423. The synchronized ELM crash is in the middle. Positive velocities correspond to the electron diamagnetic drift direction. b) Conditionally averaged spectrogram of inner vertical ECEI chord #6.

Here short, nitrogen seeded, ELMs follow each other approximately each 4.5 ms. The precursor mode appears ~ 3 ms before the crash with an initial velocity around 6 km/s in the electron diamagnetic drift direction. Then, around 1.5 ms before the crash the mode velocity pattern broadens with appearance of lower velocities and the crash follows. After the crash the mode velocity changes its rotation to the ion diamagnetic drift direction and holds the velocity of about 1 km/s during 1 ms. Then it disappears and shortly afterwards the mode reappears with the original velocity 2 ms after the crash. This mode is the ELM precursor mode for the next ELM crash. As the observed mode velocities are measured in the laboratory frame, they most probably represent the ExB velocity of the plasma as a whole, while the changes in the measured velocity reflect the changes in the radial electric field E_r. The appearance of the precursor mode is synchronised to the previous ELM crash: it appears 2 ms after, which is suggested by a very high amplitude of the corresponding spot in the conditionally averaged plot. This is probably the most interesting feature of the N_2 ELM precursor mode. Note that the precursor before the crash in the conditionally averaged plot is much less pronounced, which indicates that the time between the crash and

the next precursor is much stronger determined than the time between the precursor and the crash. Another observation is that after nitrogen puffing the ELM precursor accompanies each short ELM, but before the nitrogen is being puffed the precursor appears before the short ELMs only occasionally.

Fig. 6b shows the ELM synchronized spectrogram corresponding to the discussed precursor mode velocity. The spectrogram is averaged over all channels of the vertical chord, where the mode is seen clearest. From the figure it is seen, that the typical frequencies of the precursor mode are in the order of several kHz. Due to short duration of the precursor mode it is not possible to determine its frequency with a better resolution. The better synchronization of a precursor to the previous ELM crash rather than to the following one is also supported by the spectrogram.

5 Plasma kinetic profiles

It has been observed that nitrogen seeded ELMs cause a smaller drop in both temperature and density than type-I ELMs [13]. Fig. 7 illustrates this for AUG discharge #30423, where the plasma kinetic profiles, provided by IDA [37], are separately averaged over long and short ELMs. The red lines in Fig. 7 correspond to the profiles before and after long ELMs (solid and dashed lines correspondingly), whereas the green lines correspond to the profiles before and after short ELMs. The relative difference between the profiles before crashes and after - the temperature and the density drops - are shown by dashed lines in the bottom plots.

In both cases of long and short ELMs the maximum density drop is situated around $\rho_{\mathrm{pol}} \sim 0.97$ (Fig. 7d), corresponding to the pedestal region, while the maximum temperature drop is situated a bit deeper in the plasma: $\rho_{\mathrm{pol}} \sim 0.95$ (Fig. 7b), corresponding to the position of the pedestal top. The temperature for nitrogen seeded (short) ELMs is higher, than those for long ELMs, which is consistent with previous observations [8][11][12]. The density profile for the N_2 seeded case is not much enhanced over the non-seeded case. For both temperature and density the temperature drop caused by the short ELMs is smaller than the drop caused by long ELMs.

Using the benefits of the ECEI diagnostic it is possible to sort and average the kinetic profiles according to the number of filaments crossing the ECEI window, during a particular ELM crash. Fig. 8 shows averaged density and temperature drops caused by the ELMs with different number of filaments. There is a trend seen, which shows, that the crashes with a higher number of filaments lead to a higher drop of the temperature profile. From the density drop plot (Fig. 8b) it is only possible to conclude that the drop caused

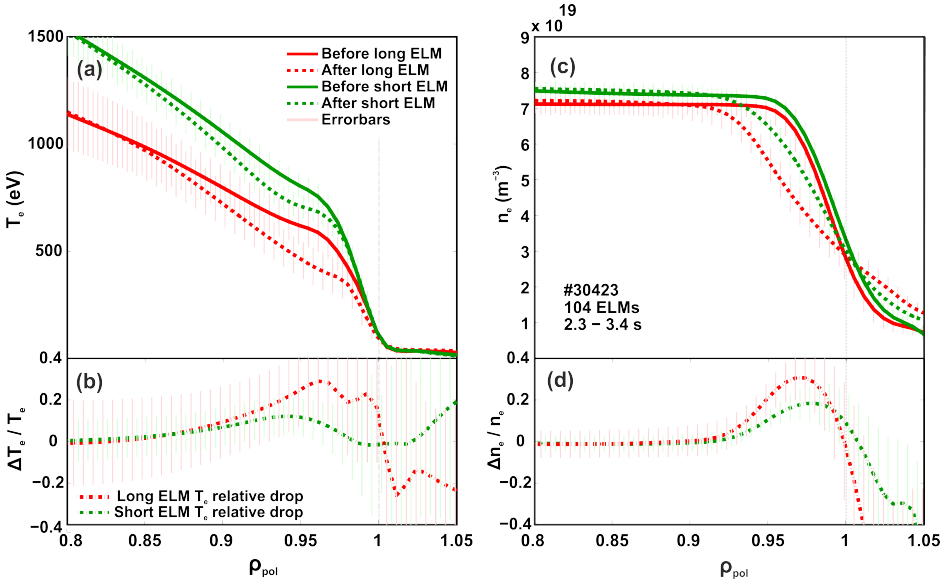

Figure 7: Averaged plasma kinetic profiles for long (red) and short (green) ELMs. Solid lines show the profiles before the crashes, whereas the dashed lines indicate the profiles after. The relative profile difference between 'before' and 'after' is plotted by the dash-dotted lines in the bottom plots.

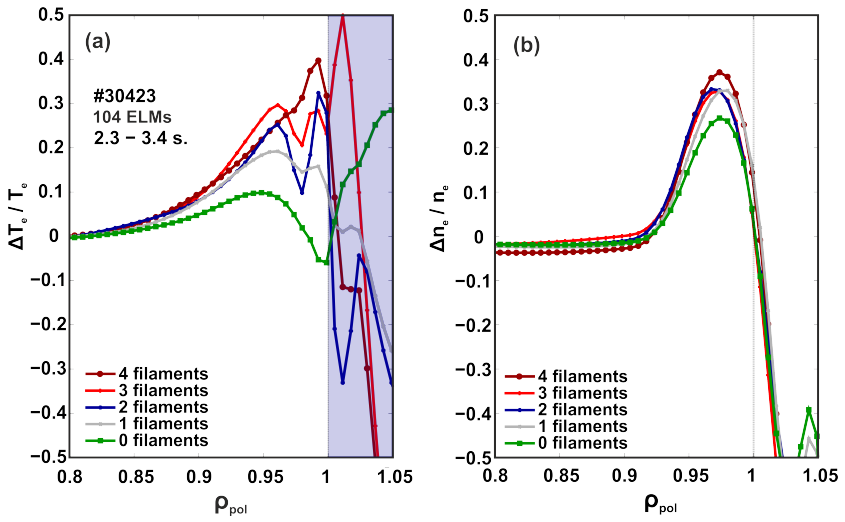

Figure 8: Relative temperature and density drops averaged by the different number of filaments, produced by the ELMs and detected by ECEI. The higher number of filaments leads to higher temperature-density drop. The data in the shaded area on the temperature plot is outside of the separatrix and is not reliable.

by the ELMs with no filaments is a bit lower. The non-smoothness of the relative temperature drops in Fig. 8a is caused by low temperature next to the separatrix (due to division by a small value: $(T_e^{\text{before}} - T_e^{\text{after}})/T_e^{\text{before}}$).

By integrating the pressure drop over the plasma volume one can obtain the amount of energy loss caused by ELMs: $\Delta E_{\text{loss}} = 3/2 \int_V 2\Delta p_e dV$. Here the ion pressure drop was taken the same as the electron pressure drop $\Delta p_i \approx \Delta p_e$ resulting in the factor of 2 under the integral sign. The integration is performed over the volume, where the profiles' change is most significant, which corresponds to the region $0.8 \leqslant \rho_{\text{pol}} \leqslant 1.0$. Calculated with this method an average energy loss per observed filament event in the analysed shots is estimated as 5 kJ, whereas the energy loss per ELM is about $30 - 40$ kJ with the total stored plasma energy of ~ 700 kJ. The relative energy loss is close to 1% of the total stored plasma energy per observed filament event or 15% of the total energy loss caused by an ELM.

In section 3 the average energy loss per filament event was calculated directly from W_{mhd} signal and was estimated as 2.5 kJ. The discrepancy between the two estimations can come from the different ways of obtaining the total stored energy W_{mhd}, high scatter in the W_{mhd} signal, not enough accurate electron temperature profiles and the small dataset on the number of filaments. Still the obtained values can be used as a rough estimate of the energy loss per filament event.

6 Summary

In the experiments conducted on AUG both long and short ELMs take place simultaneously, with the domination of long type-I ELMs, before nitrogen seeding is applied. Both types of ELMs have been characterised by ECEI. The average duration of long ELMs is $2-3$ ms, whereas for short ELMs it is 1 ms. Both groups also have different average frequencies: $100 - 150$ Hz versus $200 - 250$ Hz correspondingly. The signal of the divertor current indicates the existence of an additional phase, which is not observed for the case of short, nitrogen seeded ELMs. This phase was investigated in detail by means of the ECEI diagnostic. It was found, that in this phase some relatively hot structures with respect to the background plasma, so-called filaments, are ejected.

The channel of the additional losses in the absence of nitrogen had not been identified for a long time, however, filaments were one of the likely candidates [13]. With the help of ECEI on AUG it became possible to prove, that filaments are playing a role in these losses. Filaments only exist in the additional phase (Ib) (Fig. 3) and their number is connected to both the ELM

duration and the ELM related pressure drop. The corresponding energy loss per observed filament event for the analysed discharges is about $2.5 - 5\,\mathrm{kJ}$ or $0.5 - 1\%$ of the total stored plasma energy. The average total energy loss due to type-I ELMs is $30 - 40\,\mathrm{kJ}$. The filaments rotate in the electron diamagnetic drift direction with a typical velocity of $2\,\mathrm{km/s}$. Their lifetime is estimated to be in the range of $200 - 400\,\mu\mathrm{s}$. Filaments are not seen to be ejected in bursts, however, in the considered discharges one ELM can eject up to $4 - 5$ filaments. The short ELMs can occasionally eject one filament, but most commonly do not eject any.

As soon as there is enough nitrogen in the plasma, the number of filaments produced by each ELM reduces and subsequently ELMs become shorter. When the nitrogen puff is high enough, the long type-I ELMs completely disappear. The transition from long ELMs to the short ones under the effect of nitrogen is quite sharp and reminiscent to a ladder step.

The short nitrogen seeded ELMs are accompanied by a precursor which is typically not observed for long type-I ELMs. The precursor represents a coherent temperature fluctuation which appears 3 ms prior to the following ELM crash with which it merges. The short ELMs, which co-exist in the plasma with the long ELMs before the nitrogen is being puffed, demonstrate the precursor mode only occasionally. The precursors are most pronounced inside the separatrix, have the velocity of $\sim 6\,\mathrm{km/s}$ in the electron diamagnetic drift direction and have a frequency of several kilohertz. An interesting observation is that the time between an ELM crash and the next precursor is much stronger determined than the time between the precursor and the following crash.

The calculations performed for MAST show that lowering of the SOL temperature, amongst other effects, leads to reduction of the number of produced filaments [17]. From another side, it was experimentally observed that nitrogen reduces the temperature in the divertor and SOL regions[5][6][7]. Although on MAST the separatrix temperature is up to 10 times lower than on AUG, with the assumption that MAST calculations represent a general effect and can be extrapolated to other machines, it is possible to make a hypothesis, that nitrogen can indirectly reduce the number of filaments leading to shorter ELMs by lowering the SOL temperature. A similar modelling with use of JOREK code is planned to be performed on AUG soon.

Acknowledgments

This work has been carried out within the framework of the EUROfusion Consortium and has received funding from the Euratom research and training programme 2014-2018 under grant agreement No 633053. The views and

opinions expressed herein do not necessarily reflect those of the European Commission.

References

[1] A. Kallenbach et al. *Plasma Phys. Control. Fusion* **52** (2010) 055002

[2] M. Reinke et al. *J. Nucl. Mat.* **415** (2011) 40

[3] J. Ferron et al. *Phys. Plasmas* **7** (2000) 1976

[4] G. Jackson et al. *Nucl. Fusion* **42** (2002) 28

[5] O. Gruber et al. *Nucl. Fusion* **49** (2009) 115014

[6] C. Fuchs et al. *J. of Nucl. Mat.* **415** (2011) S852

[7] A. Kallenbach et al. *Nucl. Fusion* **49** (2009) 045007

[8] G. Tardini et al. *Plasma Phys. Control. Fusion* **55** (2013) 015010

[9] C. Giroud et al. *Nucl. Fusion* **53** (2013) 113025

[10] G. Maddison et al. *Nucl. Fusion* **54** (2014) 073016

[11] J. Schweinzer et al. *Nucl. Fusion* **51** (2011) 113003

[12] G. Maddison et al. Contrasting H-mode behaviour with fuelling and nitrogen seeding in the all-carbon and metallic versions of JET. *Proc. 40th EPS Conf. on Plasma Physics* (Helsinki, Finland, 1-5 July 2013) O2.116

[13] P. Schneider et al. *Plasma Phys. Control. Fusion* **56** (2014) 025011 (15pp)

[14] P. Schneider et al. *Plasma Phys. Control. Fusion* **57** (2015) 014029

[15] M. Dunne et al. *Nucl. Fusion* **55** (2015) 013013

[16] H. Müller et al. *Nucl. Fusion* **51** (2011) 073023

[17] S. Pamela et al. Effect of SOL Temperature on Filament Dynamics in MAST *Proc.* 41st *EPS Conf. on Plasma Physics* Berlin, Germany, 23-27 June 2014 P5.061

[18] A. Kirk et al. *Plasma Phys. Control. Fusion* **49** (2007) 1259

[19] A. Kirk et al. *J. of Phys.: Conf. Series* **123** (2008) 012011

[20] A. Herrmann et al. *J. Nucl. Mat.* **313-316** (2003) 759

[21] M. Beurskens et al. Pedestal dynamiscs in ELMy H-mode plasmas in JET, *Proc. of* 22nd *IAEA Fusion Energy Conference* Geneva, Switzerland, 2008 EX/P3-4

[22] B. LaBombard et al. *Phys. Plasmas* **2** (1995) 2242

[23] N. Ben Ayed et al. *Plasma Phys. Control. Fusion* **51** (2009) 035016

[24] G. Yun et al. *Phys. Rev. Lett.* **107** (2011) 045004

[25] I.G.J. Classen et al. *Rev. Sci. Instrum.* **81** (2010) 10D929

[26] A. Kirk et al. *J. Nucl. Mat.* **390-391** (2009) 727

[27] J. Boom et al. *Nucl. Fusion* **51** (2011) 103039

[28] A. Kallenbach et al. *Nucl. Fusion* **48** (2008) 085008

[29] A. Kirk et al. *Plasma Phys. Control. Fusion* **49** (2007) 1259

[30] R. Scannell et al. *Plasma Phys. Control. Fusion* **49** (2007) 1431

[31] A. Kirk et al. *Nucl. Fusion* **54** (2014) 114012

[32] A. Herrmann et al. *Plasma Phys. Control. Fusion* **46** (2004) 971

[33] A. Bogomolov et al. *Nucl. Fusion* **55** (2015) 083018

[34] J. Boom et al. *Nucl. Fusion* **52** (2012) 114004

[35] I. Classen et al. *Nucl. Fusion* **53** (2013) 073005

[36] R. Wenninger et al. *Nucl. Fusion* **52** (2012) 114025

[37] R. Fischer et al. *Fusion Sci. Techn.* **58/2** (2010) 675